catalysts

MDPI

Article

An Evolutionary Marker of the Ribokinase Superfamily Is Responsible for Zinc-Mediated Regulation of Human Pyridoxal Kinase

César A. Ramírez-Sarmiento [1,*], Felipe Engelberger [1] and Victoria Guixé [2,*]

[1] Institute for Biological and Medical Engineering, Schools of Engineering, Medicine and Biological Sciences, Pontificia Universidad Católica de Chile, Av. Vicuña Mackenna 4860, Santiago 7820436, Chile; felipe.engelberger@ug.uchile.cl

[2] Departamento de Biología, Facultad de Ciencias, Universidad de Chile, Las Palmeras 3425, Santiago 7800003, Chile

* Correspondence: cesar.ramirez@uc.cl (C.A.R.-S.); vguixe@uchile.cl (V.G.); Tel.: +56-2-2354-1110 (C.A.R.-S.); +56-2-2978-7335 (V.G.)

Received: 12 April 2020; Accepted: 11 May 2020; Published: 18 May 2020

Abstract: The ribokinase superfamily catalyzes the phosphorylation of a vast diversity of substrates, and its members are characterized by the conservation of a common structural fold along with highly conserved sequence motifs responsible for phosphoryl transfer (GXGD) and stabilization of the metal-nucleotide complex (NXXE). Recently, a third motif (HXE) exclusive from ADP-dependent enzymes was identified, with its glutamic acid participating in water-mediated interactions with the metal-nucleotide complex and in stabilization of the ternary complex during catalysis. In this work, we bioinformatically determine that the aspartic acid of another motif (DPV), exclusively found in hydroxyethyl thiazole (THZK), hydroxymethyl pyrimidine (HMPK) and pyridoxal kinases (PLK), is structurally equivalent to the acidic residue in the HXE motif. Moreover, this residue is highly conserved among all ribokinase superfamily members. To determine whether the functional role of the DPV motif is similar to the HXE motif, we employed molecular dynamics simulations using crystal structures of phosphoryl donor substrate-complexed THZK and PLK, showing that its aspartic acid participated in water-mediated or direct interactions with the divalent metal of the metal-nucleotide complex. Lastly, enzyme kinetic assays on human PLK, an enzyme that utilizes zinc, showed that site-directed mutagenesis of the aspartic acid from the DPV motif abolishes the inhibition of this enzyme by increasing free zinc concentrations. Altogether, our results highlight that the DPV and HXE motifs are evolutionary markers of the functional and structural divergence of the ribokinase superfamily and evidence the role of the DPV motif in the interaction with both free and nucleotide-complexed divalent metals in the binding site of these enzymes.

Keywords: pyridoxal kinase; enzyme activity; zinc regulation; metal-assisted catalysis; evolution

1. Introduction

Enzymes from the ribokinase superfamily can catalyze the phosphorylation of a wide spectrum of substrates, from sugars to nucleosides, and can be found in all three domains of life [1]. Their evolutionary relationship is mostly determined by their common Rossmann-like fold, composed of a central beta sheet with at least eight strands in a predominantly parallel disposition surrounded by α-helices [2] and a β-meander subdomain that is located on the C-termini [3].

Beyond this conserved fold, these enzymes can be classified into different groups due to structural and functional divergences within this superfamily. Structurally, enzymes with the longest sequence lengths usually possess a second domain of small size composed of a four-stranded β-sheet located over

the active site, which is relevant for catalysis [4] or oligomerization [5]. Functionally, most enzymes from *Eukarya* and *Bacteria* use ATP as the phosphoryl donor substrate, whereas enzymes from *Archaea* and some *Eukarya* rely on ADP instead and only correspond to glucokinases (GK) and phosphofructokinases (PFK) [1]. Also, ADP-dependent enzymes exhibit a topological reordering of the β-meander that is relevant for its substrate-binding mechanism [6]. Thus, the ribokinase superfamily members can be classified into three major groups: ATP-dependent sugar kinases (ribokinase family), ATP-dependent vitamin kinases, and ADP-dependent sugar kinases [1].

Given the dependence of this enzyme on ATP (or ADP) and on a divalent metal to form a metal-nucleotide complex that is the true substrate for the phosphoryl transfer reaction [7,8], two sequence motifs related to the interaction with this moiety have been found to be conserved across all superfamily members: NXXE [8,9] and GXGD [10]. However, recently a third motif was found in ADP-dependent kinases, termed HXE, which also interacts with the metal-nucleotide complex [11] and participates in stabilization of the ternary complex during the phosphorylation reaction [12].

Reasoning that the acidic residues of the different motifs involved in the interaction with the metal-nucleotide complex (NXXE, GXGD) are highly conserved among all members of this superfamily, we performed a residue conservation analysis across this superfamily to determine whether the glutamic acid residue of HXE was also conserved. On the one hand, our results show that this acidic residue is highly conserved across the ribokinase superfamily. On the other, that it is equivalent to the acidic residue of another motif, termed DPV, previously shown by multiple sequence alignments to be conserved in pyridoxal kinases (PLK) [13] and in hydroxyethyl thiazole kinases (THZK) [14] separately, and suggested to be conserved between PLK and hydroxymethyl pyrimidine kinases (HMPK) [15]. We further confirm that the DPV motif is, in fact, conserved among all ATP-dependent vitamin kinases and unique to this family within the ribokinase superfamily.

To analyze the role of this acidic residue in the function of ATP-dependent vitamin kinases, we performed molecular dynamics (MD) simulations using the solved structures of *Bacillus subtilis* THZK and sheep PLK bound to different metal-nucleotide complexes, determining that the DPV motif participates in establishing water-mediated or direct interactions with the divalent cation. Lastly, using site-directed mutagenesis and enzyme kinetics we demonstrate that the acidic residue of the DPV motif is relevant for the inhibitory effect of free Zn^{2+} concentrations on the activity of human PLK (hPLK).

2. Results and Discussion

2.1. Real-Value Evolutionary Trace (rvET) Identifies a Three-Residue Motif that Varies between the Major Ribokinase Superfamily Groups

The ribokinase superfamily is characterized by its functional diversity, being able to catalyze ATP/ADP-dependent phosphorylations of a myriad of substrates. However, all members of the superfamily are known for having a strict conservation of catalytic residues required for stabilization of the metal-nucleotide complex (NXXE) [8,9] and for directly participating in the phosphoryl transfer reaction (GXGD) [10]. Nevertheless, our group recently described that ADP-dependent kinases also present a third conserved motif known as HXE [11], and we demonstrated experimentally that its conserved glutamate participates in water-mediated interactions with the metal-nucleotide complex and in the stabilization of the phosphoryl acceptor substrate during the formation of the ternary complex [12].

Reasoning that enzymes of the other major groups of the ribokinase superfamily exhibit free divalent metal inhibition [16] or activation [8], we speculated that a motif similar to HXE should be also present in the ATP-dependent vitamin and sugar kinases. Thus, we generated a multiple sequence alignment (MSA) using 27 different enzymes from all major groups of the ribokinase superfamily (Table 1) and determined a ranking of residue conservation using real-value evolutionary trace (rvET) analysis [17]. In these analyses, scores closer to 1.0 mean higher residue conservation.

Table 1. Structures used for the structure-based sequence alignment of the ribokinase superfamily.

Enzyme	Species	PDB ID	Family	Refs.
PLK	human	2F7K	ATP-dependent vitamin kinase	[18]
PLK	*Ovis aries*	1LHP		[19]
PLK	*Escherichia coli (pdxK)*	2DDM		[20]
PLK	*Escherichia coli (pdxY)*	1TD2		[13]
PLK	*Lactobacillus plantarum*	3H74		
HMPK	*Salmonella typhimurium*	1JXH		[21]
HMPK	*Thermus thermophilus*	1UB0		
HMPK/PLK	*Bacillus subtilis*	2I5B		[15]
HMPK	*Bacteroides thetaiotaomicron*	3MBH		
THZK	*Bacillus subtilis*	1EKQ		[14]
THZK	*Pyrococcus horikoshii*	3HPD		[22]
THZK	*Enterococcus faecalis*	3DZV		
Phosphofructokinase (PFK)	*Pyrococcus horikoshii*	1U2X	ADP-dependent sugar kinase (GK/PFK)	[23]
Glucokinase (GK)	*Pyrococcus horikoshii*	1L2L		[24]
Glucokinase (GK)	*Pyrococcus furiosus*	1UA4		[25]
GK/PFK	*Methanocaldococcus jannaschii*	5OD2		[26]
Adenosine kinase	human	1BX4	ATP-dependent sugar kinase (Ribokinase family)	[27]
Putative ribokinase	*Agrobacterium tumefaciens*	2RBC		
Nucleoside kinase	*Methanocaldococcus jannaschii*	2C49		[28]
Carbohydrate kinase	*Thermotoga maritima*	1VK4		
Nucleoside kinase	*Chlorobium tepidum*	3KD6		
Ribokinase	human	2FV7		
2-keto-3-deoxygluconate kinase	*Thermotoga maritima*	2AFB		[29]
Fructokinase	*Bacteroides thetaiotaomicron*	2QHP		
Phosphofructokinase	*Listeria innocua*	3IE7		
Phosphofructokinase	*Escherichia coli (Pfk-2)*	3CQD		[3]
Putative ribokinase	*Escherichia coli*	3IN1		

Our rvET analysis revealed the expected high conservation of the NXXE and GXGD motifs across all ribokinase superfamily members analyzed herein (Figure 1A). The NXXE motif (residues 150–153 in hPLK) has rvET scores of 4.29 for the Asn residue (variability: Asn, Asp, Ser) and 2.75 for the Glu residue (variability: Glu, Asp, Ala). The GXGD motif (residues 232–235 in hPLK) has rvET scores of 1.94 for the first Gly (variability: Gly, Ala), 1.00 for the second Gly (strict conservation, no variability) and 3.66 for the Asp residue (variability: Asp, Cys). Surprisingly, the Glu residue from the HXE motif, which is conserved among the ADP-dependent enzymes from the ribokinase superfamily, also showed significant conservation across all members, with a rvET score of 3.53. This score is similar to that of the conserved residues from the known ribokinase superfamily motifs.

Visual inspection of the sequence alignment within this region (Figure 1B) shows that this residue is replaced by Asp in all ATP-dependent vitamin kinases and by Asn and Asp in ATP-dependent sugar kinases. Moreover, this residue is part of a conserved third motif in the ATP-dependent vitamin kinases, corresponding to DPV, which was previously described for PLK [13] and THZK [14] separately, and also to be conserved between HMPK and PLK [15]. In contrast, no apparent sequence-conserved motif is seen for the ATP-dependent sugar kinases (Figure 1B). It is worth noting that the conservation between the Glu residue from the ADP-dependent HXE motif and the Asp residue from the DPV motif leads to a two-residue frame shift on its sequence location. Consistently, the Asp residue of the DPV motif is the only highly conserved residue, as the residues in the second and third position of the DPV motif have scores that are similar to those observed for the highly variable residues of the NXXE and GXGD motifs (Figure 1A).

To further establish that the DPV motif enables identification of members of the ATP-dependent kinase family, we performed an extended rvET analysis on a structure-based MSA of PLK, HMPK and THZK from the UniprotKB/SwissProt database. The analysis of 93 sequences from this family (Table 2) confirmed the high conservation of the DPV motif, with the acidic residue having rvET scores similar to the conserved residues in NXXE and GXGD, and with the other two residues having even lower scores than those observed for the variable regions of the NXXE and GXGD motifs within this protein

family (Figure 1C). These results demonstrate that the DPV motif resembles the HXE motif in terms of being uniquely conserved among ATP-dependent vitamin kinases within the ribokinase superfamily and thus its presence enables the fast identification of these enzymes.

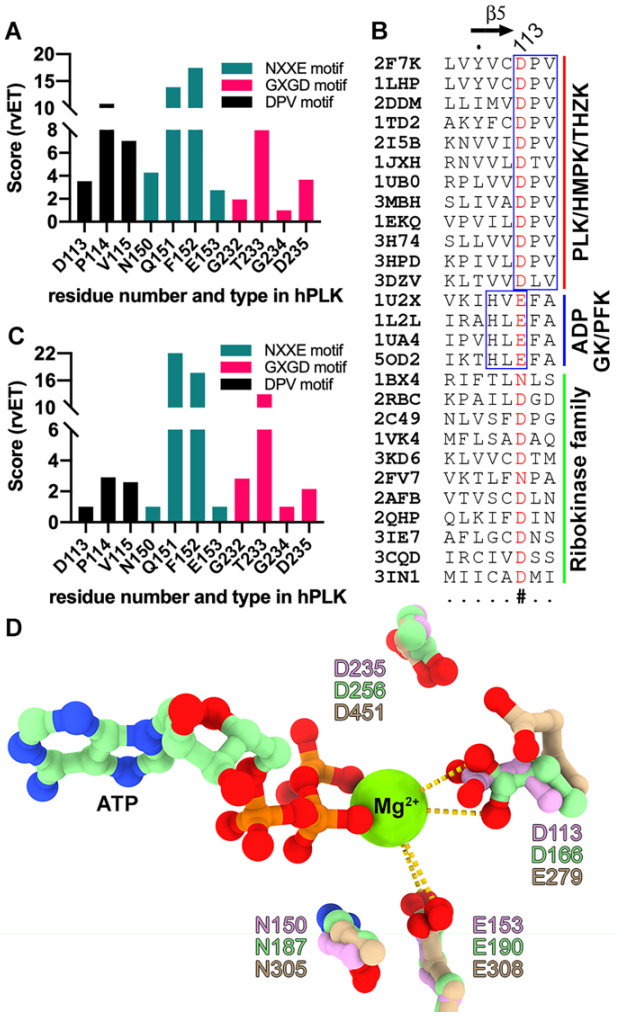

Figure 1. Identification of a third sequence motif that varies among the major groups of the ribokinase superfamily. (**A**) Real-value evolutionary trace (rvET) analysis of a structure-based multiple sequence alignment (MSA) generated for all 27 different enzymes in Table 1, representing the three major groups of the ribokinase superfamily. (**B**) MSA of the region comprising residues 108–115 of human pyridoxal kinase (hPLK) across all 27 enzymes, grouped according to the three major groups of the ribokinase superfamily. Residues with sequence conservation >70% across all enzymes are shown in red characters, whereas the HXE motif from ADP-dependent GK and PFK and the DPV motif of PLK, HMPK and THZK are shown in blue boxes. (**C**) rvET analysis of a structure-based MSA generated for 93 PLK, HMPK and THZK sequences shown in Table 2. (**D**) Stick representation of all conserved residues from the NXXE, GXGD and DPV motifs in hPLK (PDB 2F7K, pink), *E. coli* phosphofructokinase-2 (PDB 3CQD, green) and *P. horikoshii* GK (PDB 1L2L, brown). The catalytic MgATP from *E. coli* phosphofructokinase-2 is shown for reference.

Given the sequence conservation of the acidic residue from the DPV motif across all ribokinase superfamily members, we inspected its structural conservation in three different enzymes: hPLK (ATP-dependent vitamin kinases, PDB 2F7K), *E. coli* phosphofructokinase-2 (ATP-dependent sugar kinases, PDB 3CQD) and *P. horikoshii* glucokinase (ADP-dependent sugar kinases, PDB 1L2L). Structural superposition of these enzymes shows that this acidic residue is located at the end of a central β-strand of the common Rossmann-like fold (β5 in hPLK) and pointing towards the active site (Figure 1D).

Moreover, visualization of the substrates bound to *E. coli* phosphofructokinase-2 in its crystal structure shows that the acidic residue is, in fact, within coordination distance of the divalent metal placed between the β- and γ-phosphates of the metal-nucleotide complex (Figure 1D).

Altogether, these results suggest that the DPV motif is unique to all ATP-dependent vitamin kinases, and that its acidic residue is conserved across all members of the ribokinase superfamily and participates in coordination of the divalent cation from the metal-nucleotide complex.

Table 2. Sequences employed for the rvET analysis of the ATP-dependent vitamin kinase family.

Enzyme	Species	Acc. Code	Enzyme	Species	Acc. Code
THZK	*B. subtilis*	P39593	THZK	*S. epidermidis*	Q21VL4
THZK	*B. velezensis*	A7ZA59	THZK	*S. haemolyticus*	Q466J4
THZK	*B. licheniformis*	Q65DJ9	THZK	*R. ferrireducens*	Q2LWX9
THZK	*Geobacillus sp.*	C5D2N0	THZK	*M. barkeri*	B1I1S3
THZK	*B. cereus*	Q81IG9	THZK	*S. aciditrophicus*	A3CS46
THZK	*B. brevis*	C0ZGJ5	THZK	*C. Desulforudis*	Q6LPQ4
THZK	*B. pumilus*	A8FIR7	THZK	*M. marisnigri*	C0QWJ2
THZK	*G.thermodenitrificans*	A4IN26	THZK	*P. profundum*	A4J233
THZK	*A. flavithermus*	B7GKQ7	THZK	*B.hyodysenteriae*	A7IA08
THZK	*B. clausii*	Q5WDW4	THZK	*D. reducens*	Q87JW7
THZK	*Exiguobacterium sp.*	C4KZE2	HMPK	*M. boonei*	P55882
THZK	*H. somni*	Q0I129	HMPK	*V.parahaemolyticus*	P56904
THZK	*L. monocytogenes*	B8DET2	HMPK	*S. enterica*	Q6GEY2
THZK	*C. subterraneus*	Q8R807	HMPK	*S. meliloti*	P44697
THZK	*A. succinogenes*	A6VPG7	HMPK	*S. aureus*	O25515
THZK	*M. thermoacetica*	Q2RGX6	HMPK	*H. influenzae*	O31620
THZK	*H. influenzae*	Q57233	HMPK	*H. pylori*	Q9ZBR6
THZK	*D. psychrophila*	Q6AQZ6	PLK	*B. subtilis*	P77150
THZK	*T. pseudethanolicus*	B0KBA7	PLK	*S. coelicolor*	Q7N3W7
THZK	*P. multocida*	P57931	PLK	*E. coli*	Q6D5V1
THZK	*B. halodurans*	Q9K7L2	PLK	*P. laumondii*	Q66A50
THZK	*G. parasuis*	B8F7P4	PLK	*P.atrosepticum*	Q51892
THZK	*D. aliphaticivorans*	B8FJW2	PLK	*Y. pseudotuberculosis*	B7V753
THZK	*C. tetani*	Q893Q9	PLK	*P. mirabilis*	A5WB73
THZK	*M. arvoryzae*	Q0W1L9	PLK	*P. aeruginosa*	B0UUD2
THZK	*C. aggregans*	B8G7I8	PLK	*P. putida*	Q5E345
THZK	*D. oleovorans*	A8ZV98	PLK	*H. somni*	Q141E8
THZK	*S. fumaroxidans*	A0LP26	PLK	*A. fischeri*	Q65UE8
THZK	*C. beijerinckii*	A6M1W7	PLK	*P. xenovorans*	A5UA83
THZK	*B. subtilis*	B8I3J5	PLK	*M. succiniciproducens*	Q63SC2
THZK	*B. velezensis*	Q2FNE1	PLK	*H. influenzae*	A6VNE5
THZK	*R. cellulolyticum*	B2UY66	PLK	*B. pseudomallei*	Q6LP62
THZK	*M. hungatei*	A4FX33	PLK	*A. succinogenes*	Q7MGA4
THZK	*C. botulinum*	A8MK93	PLK	*P. profundum*	Q1AYE5
THZK	*M. maripaludis*	Q9UZQ4	PLK	*V. vulnificus*	Q1J237
THZK	*A. oremLandii*	B1HX32	PLK	*R. xylanophilus*	Q9RYX0
THZK	*P. abyssi*	Q8ESJ1	PLK	*D. geothermalis*	Q0BSF0
THZK	*L. sphaericus*	C1CD69	PLK	*D. radiodurans*	A8A2R4
THZK	*O. iheyensis*	Q890C2	PLK	*G. bethesdensis*	P40192
THZK	*S. pneumoniae*	Q49Z40	PLK	*E. coli*	Q7W6K7
THZK	*L. plantarum*	Q8ESZ2	PLK	*S. enterica*	Q1LFU5
THZK	*S. saprophyticus*	A5UUL2	PLK	*B. parapertussis*	Q2L1P5
THZK	*O. iheyensis*	A2SU11	PLK	*C. metallidurans*	O46560
THZK	*Roseiflexus sp.*	Q8U191	PLK	*B. avium*	Q8W1X2
THZK	*M. labreanum*	B3QT42	PLK	*S. scrofa*	O01824
THZK	*P. furiosus*	Q5HMC9	PLK	*A. thaliana*	Q55EK9
THZK	*C. thalassium*	Q4L7X4			

2.2. The DPV Motif Establishes Direct or Water-Mediated Interactions with Divalent Metals in the Active Site

Inspection of the interactions established in the active site of solved structures of PLK has shown that the aspartic acid of the DPV motif participates in either direct or water-mediated interactions with the γ-phosphate [13,20] and with monovalent cations [19,30]. In the case of ADP-dependent glucokinases, MD simulations showed the formation of water-mediated interactions between the equivalent HXE motif and the divalent cation in the metal-nucleotide complex [11].

In order to further establish the role of the DPV motif in interacting with the metal-nucleotide complex, MD simulations were performed using two of the few structures from ATP-dependent vitamin kinases that have been solved with substrates bound in their active sites. These structures correspond to THZK from *Bacillus subtilis* (PDB 1ESQ, bound to MgATP) and sheep PLK (PDB 1LHR, bound to ZnATP).

These simulations were performed in explicit solvent, and the protonation state of the different residues was assigned to pH 6.5 based on optimal enzyme activity conditions determined for other enzymes, such as hPLK, in previous works [16].

The results from 3 independent 50 ns production runs for both *B. subtilis* THZK and sheep PLK are summarized in Figure 2. For the THZK trimer, all 3 simulations showed that the Asp residue of the DPV motif (D94 for *B. subtilis* THZK) interacts with the Mg^{2+} ion from the MgATP complex in at least two subunits (Figure 2A). Moreover, this interaction is established via up to two water molecules that constitute the first coordination sphere of this ion (Figure 2B). Regardless of the continuous exchange of these water molecules throughout the simulation (data not shown), they form hydrogen bonds with the Asp residue of the DPV motif as soon as they become part of the coordination sphere of the divalent metal.

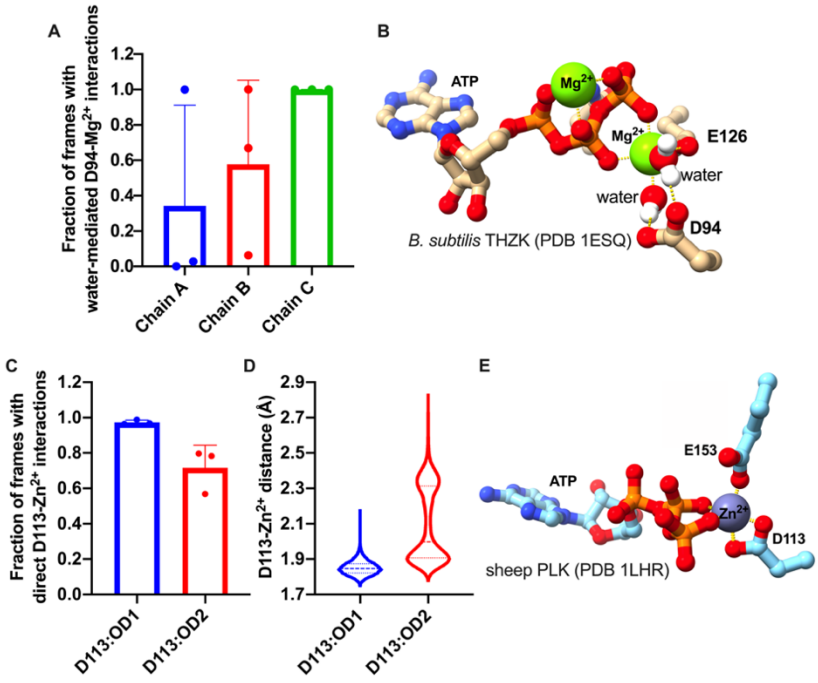

Figure 2. Role of the DPV motif in coordination of divalent metals. (**A**) Counting of water-mediated interactions between D94 and Mg^{2+} from the MgATP complex in *B. subtilis* THZK. Dots represent the fraction of frames for each MD simulation. (**B**) Stick representation of the interactions between D94 from DPV and E126 from NXXE with MgATP. (**C**) Counting of direct interactions (<2 Å) between D113 and Zn^{2+} from the ZnATP complex in sheep PLK. Dots represent the fraction of frames for each MD simulation. (**D**) Violin plot of the distance distribution between D113 and Zn^{2+}. (**E**) Stick representation of the interactions between D113 from DPV and E153 from NXXE with ZnATP.

In the case of sheep PLK, we observed that both oxygens from the carboxylic sidechain of D113 in the DPV motif are located, for the majority of the MD simulation, within 2 Å of the Zn^{2+} from the metal-nucleotide complex (Figure 2C,D). In fact, the double-bonded oxygen (OD1) from the carboxylic group of D113 stably interacts with the Zn^{2+} throughout the whole simulation, whereas its single-bonded oxygen (OD2) can reach distances up to 2.8 Å (Figure 2D) due to the participation of water molecules in establishing interactions with the phosphoryl donor substrate (data not shown). Thus, the DPV motif is participating in direct interactions with the ZnATP substrate in sheep PLK, similar to the conserved residues from the NXXE motif (Figure 2E).

Altogether, our MD simulations suggests that the DPV motif participates in either direct or water-mediated interactions with the divalent cation in the metal nucleotide complex, in agreement with previous discoveries using similar strategies for the HXE motif in ADP-dependent kinases [11].

2.3. DPV Motif is Responsible for the Free Divalent Cation Inhibition of Human Pyridoxal Kinase (hPLK)

Our previous work on the HXE and NXXE motifs from the ADP-dependent GK from *T. litoralis* showed that the HXE motif was responsible for the stabilization of the acceptor substrate during formation of the ternary complex, whereas the NXXE motif was responsible for the free Mg2+ inhibition of the activity of this enzyme [12].

Due to the sequence and structural conservation of the acidic residues from the HXE and DPV motifs between the ADP-dependent sugar kinases and ATP-dependent vitamin kinases from the ribokinase superfamily (Figure 1), we decided to explore the role of the DPV motif through site-directed mutagenesis of its Asp residue followed by enzyme kinetics.

Given the need of an appropriate model for testing the inhibitory effects of free divalent cations on enzyme activity, we opted to use hPLK, which we previously characterized to exhibit optimal *in vitro* activity using Zn^{2+} as divalent metal for the metal–nucleotide complex, but is also inhibited by increasing free Zn^{2+} concentrations [16]. Thus, we generated the site-directed mutants D113N and D113V, to evaluate the effects of eliminating the negative charge (in the case of D113N) and both the charge and volume (in the case of D113V) of the side chain of the Asp residue on the kinetic parameters and the free Zn^{2+} inhibition of this enzyme.

It is worth noting that, while the physiological role of zinc and magnesium as the preferred divalent cation for the activity of hPLK has been extensively debated [16,31], we opted to use zinc due to the availability of a thorough description of the roles exerted by all involved species (Zn^{2+}, ATP and ZnATP) in the *in vitro* activity of hPLK [16]. Moreover, similar protein-ATP interactions, including those involving the DPV motif, are observed in PLK regardless of the divalent cation present in the active site [19,30]. Therefore, the catalytic activity of hPLK and its regulation by zinc constitutes a more amenable *in vitro* kinetic model to describe the effects of mutating the DPV motif.

We determined the kinetic parameters of hPLK under two free Zn^{2+} concentrations, corresponding to low (0.1 mM) and high (0.5 mM) inhibitory effects on its enzyme activity, and saturating co-substrate concentrations (Table 3). In the case of wild-type hPLK, the apparent K_M ($K_{M,app}$) for both pyridoxal and ZnATP increases almost 3-fold due to the increase in free Zn^{2+}, while the V_{max} is similar between both conditions. However, it is worth noting that in our experimental setup, pyridoxal becomes insoluble at concentrations higher than 10 mM, and thus the V_{max} could be overestimated due to the increase in $K_{M,app}$ for pyridoxal at 0.5 mM free Zn^{2+}.

Table 3. Kinetic parameters for wild type hPLK and D113N and D113V mutants.

Free Zn^{2+}	hPLK		D113N		D113V	
	0.1 mM	**0.5 mM**	**0.1 mM**	**0.5 mM**	**0.1 mM**	**0.5 mM**
$K_{M,app}$, pyridoxal (mM)	1.44 ± 0.35	4.09 ± 0.76	0.55 ± 0.10	0.11 ± 0.03	2.34 ± 0.55	1.08 ± 0.12
$K_{M,app}$, ZnATP (μM)	20 ± 2	57 ± 12	36 ± 5	8 ± 1	13 ± 1	5 ± 1
V_{max} (μmol·min^{-1}·mg^{-1})	0.62 ± 0.04	0.70 ± 0.06	1.28 ± 0.06	0.66 ± 0.03	0.85 ± 0.08	0.77 ± 0.03

In contrast, both the D113N and D113V mutant exhibit a decrease in $K_{M,app}$ for both pyridoxal and ZnATP upon increasing the free Zn^{2+} concentrations (Table 3). While differences in $K_{M,app}$ parameters observed at low free Zn^{2+} are not significant, the D113N exhibits a $K_{M,app}$ for pyridoxal and ZnATP that is 40-fold and 7-fold lower, respectively, than the $K_{M,app}$ of the wild-type enzyme for both substrates at 0.5 mM free Zn^{2+}. Strikingly, the D113N mutant also possesses a higher V_{max} than the wild-type enzyme at 0.1 mM free Zn^{2+} and a similar V_{max} at 0.5 mM free Zn^{2+}, thus suggesting a relief in the inhibitory effect of the free divalent cation at low concentrations. For D113V, only a 4-fold decrease in the $K_{M,app}$ for pyridoxal is observed between the wild-type and mutant enzyme at 0.5 mM free Zn^{2+}, whereas the decrease in the $K_{M,app}$ for ZnATP is similar to that of D113N.

The changes observed in $K_{M,app}$ for both pyridoxal and ZnATP suggest, on the one hand, that mutations of the DPV motif affect the accommodation of both phosphoryl donor and acceptor substrates on the active site of hPLK, which is in good agreement with the effect of mutations of the HXE motif on the ADP-dependent GK from *T. litoralis* [12]. On the other hand, the increase in V_{max} for the D113N at 0.1 mM free Zn^{2+} suggest that the DPV motif also relevant for the inhibitory effect of free Zn^{2+} on the activity of hPLK, in contrast to the HXE motif in ADP-dependent sugar kinases [12]. Due to the low solubility of pyridoxal at concentrations above 10 mM under our experimental conditions, demonstration of the role of the DPV motif on ternary complex formation is challenging. In consequence, we decided to determine the specific activity of hPLK and the DPV mutants as a function of free Zn^{2+}.

Our results on hPLK resemble our previous observations [16], demonstrating that free Zn^{2+} is a potent inhibitor with a half maximal inhibitory concentration (IC_{50}) of 107 ± 16 µM (Figure 3A). The small variation in IC_{50} between our previous work and our current experiments is largely due to the use of higher concentrations of pyridoxal (6 mM), which also exerts substrate inhibition on hPLK, but that was necessary to ensure saturating conditions for all mutants under the different concentrations of free Zn^{2+} assayed in this experiment.

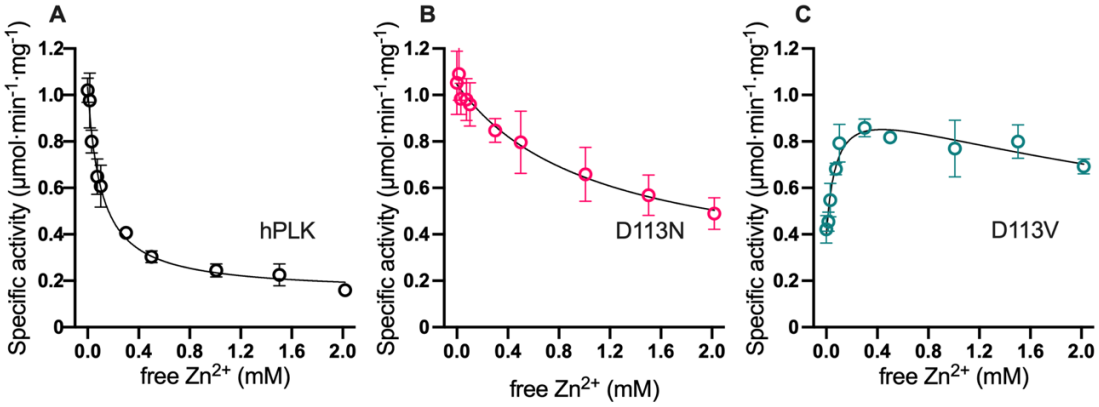

Figure 3. Effect of free Zn^{2+} concentration on the activity of hPLK and DPV mutants. (**A**) Inhibitory effect of free Zn^{2+} on wild type hPLK. (**B**) Inhibitory effect of free Zn^{2+} on D113N mutant. (**C**) Inhibitory effect of free Zn^{2+} on D113V mutant.

In the case of D113N, our results confirm the relief of the inhibitory effect of free Zn^{2+} on the activity of this mutant, with an IC_{50} of 1084 ± 337 µM (Figure 3B). Strikingly, the D113V now becomes activated by free Zn^{2+} below 0.4 mM, and then partially inhibited at higher concentrations (Figure 3C). Fitting the data to a bell-shaped stimulation curve enabled us to determine the half maximal effective concentration (EC_{50}), corresponding to 79 ± 35 µM, whereas the IC_{50} above 0.40 mM free Zn^{2+} falls outside the concentration range ascertained in this experiment.

3. Materials and Methods

3.1. Evolutionary Trace Analysis

To identify the most conserved residues throughout the ribokinase superfamily, an MSA was constructed based on the representative crystal structures from all three major structurally and functionally differentiable groups within this superfamily: ATP-dependent sugar kinases (ribokinase family), ATP-dependent vitamin kinases, and ADP-dependent sugar kinases [1]. For this analysis we selected at least one member of each clade within the previously published dendrogram of the ATP-dependent sugar kinases [32] and almost all non-redundant structures of ADP-dependent kinases, corresponding to glucokinases (GK) and phosphofructokinases (PFK), and ATP-dependent vitamin kinases, corresponding to pyridoxal (PLK), hydroxymethyl pyrimidine (HMPK) and hydroxyethyl thiazole kinases (THZK) (Table 1).

These structures were used as three-dimensional constraints for obtaining a structure-based MSA using the PROMALS3D server [33], which was then manually corrected. The final MSA, containing the sequences of all 27 selected structures, was submitted into the Universal Evolutionary Trace server [34] to obtain a ranking of residues by conservation across all sequences based on the rvET metric [17].

To determine the most conserved residues within the binding site of the group of ATP-dependent vitamin kinases, a real-value evolutionary trace (rvET) analysis was also performed. Briefly, sequences of representative structures of PLK (PDB 2F7K, 2DDM, 1TD2), HMPK (PDB 1JXH) and THZK (PDB 1EKQ) were used as query to retrieve the sequences of homologous enzymes from the UniProtKB/Swiss-Prot [35] database with 40%–80% sequence identity and >90% sequence coverage using BLAST [36]. The resulting sequences from these multiple searches were combined and then clustered based on an 80% sequence identity cut-off using the CD-HIT webserver [37]. The clustered sequences were then aligned using the PROMALS3D server [33], using the solved structures of PLK, HMPK and THZK in Table 1 to provide structural alignment-based constraints, resulting in an MSA that was manually filtered to eliminate sequences introducing long gaps. The manually curated MSA, containing 93 sequences (Table 2) was analyzed on the Universal Evolutionary Trace server [34] to obtain the rvET ranking of residue conservation.

3.2. Molecular Dynamics

To establish the role of the DPV motif in ligand binding, we performed explicit solvent molecular dynamics (MD) simulations using the crystal structures of the trimeric THZK from *Bacillus subtilis* with bound MgATP (PDB 1ESQ [14]) and a monomer of sheep PLK with bound ZnATP (PDB 1LHR [19]) as initial coordinates. Missing residues in 1ESQ were added using the software MODELLER [38]. The decision to use a monomer for sheep PLK was based on previous works indicating that this enzyme can dissociate from the dimer seen in the crystal structure into active monomers below 2 mg/mL [39].

Simulations were carried out using the Amber16 suite (Amber Software, San Francisco, CA, USA) [40] along with the AMBERff14SB force field [41] and ATP parameters obtained from the Bryce AMBER Parameter Database [42]. For each protein, the protonation state of the residues at pH 6.5 were estimated using the H++ server [43] and then a simulation system with 1.8 nm (1ESQ) or 1.7 nm (1LHR) of padding was set, filled with TIP3P water molecules and neutralized with counter ions. Each system was first minimized using the steepest descent method with position restraints on water and ions, followed by a second minimization without any position restraints. Then, the protein atoms in each system were equilibrated at 298 K for 60 ps at constant volume using a Langevin thermostat, followed by equilibration of the solvent atoms of each system for 2 ns at 298 K and constant pressure of 1 bar using a Berendsen barostat until density was stable, upon which a third and final equilibration step of the whole system for 2 ns under the same temperature and pressure conditions was performed. Production MD runs were carried out in three replicas for 50 ns each, using a timestep of 2.0 fs alongside the SHAKE algorithm and the particle mesh Ewald method for long-range electrostatics, with a 10 A

cutoff for short-range electrostatics. Independent runs were ensured by using random seeds for initial velocities during the equilibration step.

Interactions between the aspartic acid from the DPV motif and other atoms within the system were analyzed using the *cpptraj* module of AMBER16 [44]. For hydrogen bonds, donor and acceptor interactions between water molecules surrounding the metal-ATP complex during the simulation and the aspartic acid of the DPV motif were determined using a 3.5 Å cutoff. For direct divalent metal-aspartate interactions, distance cutoffs were specified based on the atom–atom distances observed during the MD simulations.

3.3. Overexpression and Purification of hPLK

Wild type hPLK and the D113N and D113V mutants were recombinantly overexpressed and purified as in previous works [16]. Briefly, kanamycin-resistant pET-28a plasmids encoding each N-terminal histidine-tagged enzyme were transformed into *E. coli* BL21 (DE3) cells. Bacteria were grown in kanamycin-supplemented Terrific Broth medium at 37 °C and protein expression was induced overnight by adding 1 mM isopropyl-β-D-thiogalactopyranoside (IPTG) upon reaching an optical density at 600 nm of 0.6–0.7. Cells were harvested by centrifugation, resuspended in binding buffer (50 mM Tris-HCl pH 7.6, 5 mM MgCl2, 5% glycerol, 0.5 M NaCl, 1 mM dithiothreitol, 5 mM imidazole) and lysed by sonication. Cleared lysates were loaded onto a Ni-Sepharose column (GE Healthcare Bio-Sciences, Pittsburgh, PA, USA), washed with 10 volumes of binding buffer containing 50 mM imidazole, and then eluted with the same buffer containing 300 mM imidazole. Active fractions were pooled and dialyzed against 50 mM Tris-HCl pH 7.6, 5% glycerol, 0.5 M NaCl, 1 mM dithiothreitol. Lastly, the protein was concentrated, supplemented with 5 mM MgCl2 and stored at a concentration of 2 mg/mL in 50% glycerol at −20 °C. The purity and homogeneity of the protein solution was verified using sodium dodecyl-sulfate polyacrylamide gel electrophoresis (SDS-PAGE), whereas protein concentration was determined through a Bradford assay, using bovine serum albumin as standard [45].

3.4. Enzyme Activity Assays

The activity of hPLK was measured spectrophotometrically as in our previous works [16]. Enzyme assays were initiated by adding 0.18 μM of purified hPLK to an assay mixture containing 20 mM PIPES pH 6.5, pyridoxal, ATP and $ZnCl_2$ at 37 °C and reactions were incubated for 5 min. Formation of product pyridoxal-5′-phosphate (PLP) was quantified based on the absorbance change at 388 nm where PLP is known to have its maximum absorption with an extinction coefficient of 4900 $M^{-1}cm^{-1}$ at pH 7.0.

Varying ATP and $ZnCl_2$ concentrations were employed to change the amount of free Zn^{2+}, which acts as an inhibitor of hPLK [16], while keeping the concentration of ZnATP constant, based on the association constant for the respective metal-nucleotide complex at 37 °C ($K_a = 5.47 \times 10^{-4}$ M^{-1} [46]). Calculation of species in solution with respect to the solution pH was performed according to the method described by Cornish-Bowden and Storer [47] as in our previous works [16].

Initial velocity data were employed for non-linear fitting to the Michaelis–Menten equation to estimate apparent kinetic constants ($K_{M,app}$) for pyridoxal and ZnATP and the catalytic constant (*kcat*) of production formation under saturating substrate conditions (6 mM pyridoxal, 2 mM ZnATP). Enzyme activity as a function of free Zn^{2+} was fitted according to a dose-response inhibition curve or a bell-shaped stimulation curve in which low doses activate the enzyme and high doses inhibit the enzyme.

4. Conclusions

By employing a residue conservation analysis on several members of the ribokinase superfamily, we were able to determine the presence of a third motif, termed DPV, that is exclusively conserved in all ATP-dependent vitamin kinases from the ribokinase superfamily (Figure 1). Interestingly, the acidic

residue of this motif is equivalent to the glutamic acid in the HXE motif of ADP-dependent sugar kinases and is highly conserved across all ribokinase superfamily members considered in this analysis.

The presence of the mutually exclusive conservation of the HXE and DPV motifs in two of the three major groups of the ribokinase superfamily, and the absence of an equivalent motif in the ATP-dependent sugar kinases, could be partly explained due to the structural, evolutionary and metabolic relationships within each group. For ADP-dependent sugar kinases, the enzymes correspond to GK and PFK that participate in the Embden–Meyerhof pathway for the utilization of glucose [1] and are the only known members that contain the topological rewiring of the β-meander in the C-termini [6]. Also, enzymes with bifunctional activity have been described to emerge or disappear during the evolution of this protein family [48]. For ATP-dependent vitamin kinases, these enzymes not only correspond to the smallest members of the ribokinase superfamily [14], but it also has been demonstrated that some HMPK are also able to phosphorylate pyridoxal due to their emergence from an ancestral enzyme with catalytic promiscuity for this substrate [49]. In terms of metabolic relationships, both THZK and HMPK participate in thyamine biosynthesis [50], while PLK participates in the vitamin B6 salvage pathway [51]. These evolutionary, structural and metabolic relationships are not obvious in the group of ATP-dependent sugar kinases.

Our computational and experimental results also provide sufficient evidence of the role of the DPV motif in interacting with the metal-nucleotide complexes in the active site of ATP-dependent vitamin kinases and thus in shaping their catalytic and regulatory features. In particular for hPLK, the DPV motif participates in regulating the inhibition of this enzyme by free zinc concentrations. This is a stark contrast with the role of the equivalent HXE and NXXE motifs in ADP-dependent sugar kinases, in which it is the NXXE motif that participates in the inhibitory effect of free divalent metals [12]. Considering that not all ribokinase superfamily enzymes are inhibited by free divalent metals [11] and that some enzymes, including hPLK, can be also activated by other monovalent or divalent cations [30,31], these results suggest that there is an interesting plasticity in the role of the cation-interacting motifs within the ribokinase superfamily and in how these motifs are related to the varying effects exerted by different cations that remains unexplored.

Altogether, the DPV motif, along with the HXE motif from the ADP-dependent kinases, enables us to dissect the ribokinase superfamily in its three major groups (either due to their conservation or their absence), thus constituting a catalytically relevant evolutionary marker of the structural and functional divergence within this superfamily.

Author Contributions: Conceptualization, C.A.R.-S. and V.G.; methodology, C.A.R.-S; formal analysis, C.A.R.-S. and F.E.; investigation, C.A.R.-S. and F.E.; data curation, C.A.R.-S.; writing—original draft preparation, C.A.R.-S. and V.G.; writing—review and editing, C.A.R.-S. and V.G.; supervision, V.G.; funding acquisition, V.G. All authors have read and agreed to the published version of the manuscript.

Funding: This research was funded by grants from Fondo Nacional de Desarrollo Científico y Tecnológico (Fondecyt 1110137, 1150460 and 1191321).

Acknowledgments: This research was partially supported by the supercomputing infrastructure of the NLHPC (ECM-02).

Conflicts of Interest: The authors declare no conflict of interest.

References

1. Guixé, V.; Merino, F. The ADP-dependent sugar kinase family: Kinetic and evolutionary aspects. *IUBMB Life* **2009**, *61*, 753–761. [CrossRef]
2. Sigrell, J.A.; Cameron, A.D.; Jones, T.A.; Mowbray, S.L. Structure of Escherichia coli ribokinase in complex with ribose and dinucleotide determined to 1.8 å resolution: Insights into a new family of kinase structures. *Structure* **1998**, *6*, 183–193. [CrossRef]
3. Cabrera, R.; Ambrosio, A.L.B.; Garratt, R.C.; Guixé, V.; Babul, J. Crystallographic Structure of Phosphofructokinase-2 from Escherichia coli in Complex with Two ATP Molecules. Implications for Substrate Inhibition. *J. Mol. Biol.* **2008**, *383*, 588–602. [CrossRef] [PubMed]

4. Rivas-Pardo, J.A.; Alegre-Cebollada, J.; Ramírez-Sarmiento, C.A.; Fernandez, J.M.; Guixé, V. Identifying Sequential Substrate Binding at the Single-Molecule Level by Enzyme Mechanical Stabilization. *ACS Nano* **2015**, *9*, 3996–4005. [CrossRef] [PubMed]
5. Ramírez-Sarmiento, C.A.; Baez, M.; Zamora, R.A.; Balasubramaniam, D.; Babul, J.; Komives, E.A.; Guixé, V. The Folding Unit of Phosphofructokinase-2 as Defined by the Biophysical Properties of a Monomeric Mutant. *Biophys. J.* **2015**, *108*, 2350–2361. [CrossRef]
6. Herrera-Morande, A.; Castro-Fernández, V.; Merino, F.; Ramírez-Sarmiento, C.A.; Fernández, F.J.; Vega, M.C.; Guixé, V. Protein topology determines substrate-binding mechanism in homologous enzymes. *Biochim. Biophys. Acta Gen. Subj.* **2018**, *1862*, 2869–2878. [CrossRef]
7. Maj, M.C.; Singh, B.; Gupta, R.S. Pentavalent ions dependency is a conserved property of adenosine kinase from diverse sources: Identification of a novel motif implicated in phosphate and magnesium ion binding and substrate inhibition. *Biochemistry* **2002**, *41*, 4059–4069. [CrossRef]
8. Parducci, R.E.; Cabrera, R.; Baez, M.; Guixé, V. Evidence for a catalytic Mg2+ ion and effect of phosphate on the activity of Escherichia coli phosphofructokinase-2: Regulatory properties of a ribokinase family member. *Biochemistry* **2006**, *45*, 9291–9299. [CrossRef]
9. Quiroga-Roger, D.; Babul, J.; Guixé, V. Role of monovalent and divalent metal cations in human ribokinase catalysis and regulation. *BioMetals* **2015**, *28*, 401–413. [CrossRef]
10. Gandhi, A.K.; Ghatge, M.S.; Musayev, F.N.; Sease, A.; Aboagye, S.O.; di Salvo, M.L.; Schirch, V.; Safo, M.K. Kinetic and structural studies of the role of the active site residue Asp235 of human pyridoxal kinase. *Biochem. Biophys. Res. Commun.* **2009**, *381*, 12–15. [CrossRef]
11. Merino, F.; Rivas-Pardo, J.A.; Caniuguir, A.; García, I.; Guixé, V. Catalytic and regulatory roles of divalent metal cations on the phosphoryl-transfer mechanism of ADP-dependent sugar kinases from hyperthermophilic archaea. *Biochimie* **2012**, *94*, 516–524. [CrossRef] [PubMed]
12. Abarca-Lagunas, M.J.; Rivas-Pardo, J.A.; Ramírez-Sarmiento, C.A.; Guixé, V. Dissecting the functional roles of the conserved NXXE and HXE motifs of the ADP-dependent glucokinase from *Thermococcus litoralis*. *FEBS Lett.* **2015**, *589*, 3271–3276. [CrossRef] [PubMed]
13. Safo, M.K.; Musayev, F.N.; Hunt, S.; di Salvo, M.L.; Scarsdale, N.; Schirch, V. Crystal structure of the PdxY Protein from Escherichia coli. *J. Bacteriol.* **2004**, *186*, 8074–8082. [CrossRef] [PubMed]
14. Campobasso, N.; Mathews, I.I.; Begley, T.P.; Ealick, S.E. Crystal Structure of 4-Methyl-5-β-hydroxyethylthiazole Kinase from Bacillus subtilis at 1.5 Å Resolution. *Biochemistry* **2000**, *39*, 7868–7877. [CrossRef]
15. Newman, J.A.; Das, S.K.; Sedelnikova, S.E.; Rice, D.W. The Crystal Structure of an ADP Complex of Bacillus subtilis Pyridoxal Kinase Provides Evidence for the Parallel Emergence of Enzyme Activity During Evolution. *J. Mol. Biol.* **2006**, *363*, 520–530. [CrossRef]
16. Navarro, F.; Ramírez-Sarmiento, C.A.; Guixé, V. Catalytic and regulatory roles of species involved in metal–nucleotide equilibriums in human pyridoxal kinase. *BioMetals* **2013**, *26*, 805–812. [CrossRef]
17. Mihalek, I.; Reš, I.; Lichtarge, O. A Family of Evolution–Entropy Hybrid Methods for Ranking Protein Residues by Importance. *J. Mol. Biol.* **2004**, *336*, 1265–1282. [CrossRef]
18. Cao, P.; Gong, Y.; Tang, L.; Leung, Y.-C.; Jiang, T. Crystal structure of human pyridoxal kinase. *J. Struct. Biol.* **2006**, *154*, 327–332. [CrossRef]
19. Li, M.H.; Kwok, F.; Chang, W.R.; Lau, C.K.; Zhang, J.P.; Lo, S.C.L.; Jiang, T.; Liang, D.C. Crystal structure of brain pyridoxal kinase, a novel member of the ribokinase superfamily. *J. Biol. Chem.* **2002**, *277*, 46385–46390. [CrossRef]
20. Safo, M.K.; Musayev, F.N.; di Salvo, M.L.; Hunt, S.; Claude, J.-B.; Schirch, V. Crystal Structure of Pyridoxal Kinase from the Escherichia coli pdxK Gene: Implications for the Classification of Pyridoxal Kinases. *J. Bacteriol.* **2006**, *188*, 4542–4552. [CrossRef]
21. Cheng, G.; Bennett, E.M.; Begley, T.P.; Ealick, S.E. Crystal structure of 4-amino-5-hydroxymethyl-2-methylpyrimidine phosphate kinase from Salmonella typhimurium at 2.3 Å resolution. *Structure* **2002**, *10*, 225–235. [CrossRef]
22. Jeyakanthan, J.; Thamotharan, S.; Velmurugan, D.; Rao, V.S.N.; Nagarajan, S.; Shinkai, A.; Kuramitsu, S.; Yokoyama, S. New structural insights and molecular-modelling studies of 4-methyl-5-β-hydroxyethylthiazole kinase from Pyrococcus horikoshii OT3 (Ph ThiK). *Acta Crystallogr. Sect. F Struct. Biol. Cryst. Commun.* **2009**, *65*, 978–986. [CrossRef] [PubMed]

23. Currie, M.A.; Merino, F.; Skarina, T.; Wong, A.H.Y.; Singer, A.; Brown, G.; Savchenko, A.; Caniuguir, A.; Guixé, V.; Yakunin, A.F.; et al. ADP-dependent 6-Phosphofructokinase from Pyrococcus horikoshii OT3. *J. Biol. Chem.* **2009**, *284*, 22664–22671. [CrossRef] [PubMed]
24. Tsuge, H.; Sakuraba, H.; Kobe, T.; Kujime, A.; Katunuma, N.; Ohshima, T. Crystal structure of the ADP-dependent glucokinase from Pyrococcus horikoshii at 2.0-Å resolution: A large conformational change in ADP-dependent glucokinase. *Protein Sci.* **2009**, *11*, 2456–2463. [CrossRef] [PubMed]
25. Ito, S.; Fushinobu, S.; Jeong, J.J.; Yoshioka, I.; Koga, S.; Shoun, H.; Wakagi, T. Crystal structure of an ADP-dependent glucokinase from Pyrococcus furiosus: Implications for a sugar-induced conformational change in ADP-dependent kinase. *J. Mol. Biol.* **2003**, *331*, 871–883. [CrossRef]
26. Tokarz, P.; Wiśniewska, M.; Kamiński, M.M.; Dubin, G.; Grudnik, P. Crystal structure of ADP-dependent glucokinase from Methanocaldococcus jannaschii in complex with 5-iodotubercidin reveals phosphoryl transfer mechanism. *Protein Sci.* **2018**, *27*, 790–797. [CrossRef]
27. Mathews, I.I.; Erion, M.D.; Ealick, S.E. Structure of human adenosine kinase at 1.5 Å resolution. *Biochemistry* **1998**, *37*, 15607–15620. [CrossRef]
28. Arnfors, L.; Hansen, T.; Schönheit, P.; Ladenstein, R.; Meining, W. Structure of Methanocaldococcus jannaschii nucleoside kinase: An archaeal member of the ribokinase family. *Acta Crystallogr. Sect. D Biol. Crystallogr.* **2006**, *62*, 1085–1097. [CrossRef]
29. Mathews, I.I.; McMullan, D.; Miller, M.D.; Canaves, J.M.; Elsliger, M.-A.; Floyd, R.; Grzechnik, S.K.; Jaroszewski, L.; Klock, H.E.; Koesema, E.; et al. Crystal structure of 2-keto-3-deoxygluconate kinase (TM0067) from Thermotoga maritima at 2.05 Å resolution. *Proteins Struct. Funct. Bioinforma.* **2007**, *70*, 603–608. [CrossRef]
30. Musayev, F.N.; di Salvo, M.L.; Ko, T.-P.; Gandhi, A.K.; Goswami, A.; Schirch, V.; Safo, M.K. Crystal Structure of human pyridoxal kinase: Structural basis of M + and M 2+ activation. *Protein Sci.* **2007**, *16*, 2184–2194. [CrossRef]
31. Di Salvo, M.L.; Hunt, S.; Schirch, V. Expression, purification, and kinetic constants for human and Escherichia coli pyridoxal kinases. *Protein Expr. Purif.* **2004**, *36*, 300–306. [CrossRef] [PubMed]
32. Cabrera, R.; Babul, J.; Guixé, V. Ribokinase family evolution and the role of conserved residues at the active site of the PfkB subfamily representative, Pfk-2 from Escherichia coli. *Arch. Biochem. Biophys.* **2010**, *502*, 23–30. [CrossRef] [PubMed]
33. Pei, J.; Grishin, N.V. PROMALS3D: Multiple Protein Sequence Alignment Enhanced with Evolutionary and Three-Dimensional Structural Information. In *Multiple Sequence Alignment Methods*; Humana Press: Totowa, NJ, USA, 2014; Volume 1079, pp. 263–271. ISBN 978-1-62703-646-7.
34. Lua, R.C.; Wilson, S.J.; Konecki, D.M.; Wilkins, A.D.; Venner, E.; Morgan, D.H.; Lichtarge, O. UET: A database of evolutionarily-predicted functional determinants of protein sequences that cluster as functional sites in protein structures. *Nucleic Acids Res.* **2016**, *44*, D308–D312. [CrossRef] [PubMed]
35. Boutet, E.; Lieberherr, D.; Tognolli, M.; Schneider, M.; Bansal, P.; Bridge, A.J.; Poux, S.; Bougueleret, L.; Xenarios, I. UniProtKB/Swiss-Prot, the Manually Annotated Section of the UniProt KnowledgeBase: How to Use the Entry View. In *Methods in Molecular Biology*; Humana Press: New York, NY, USA, 2016; pp. 23–54.
36. Zhang, Z.; Schäffer, A.A.; Miller, W.; Madden, T.L.; Lipman, D.J.; Koonin, E.V.; Altschul, S.F. Protein sequence similarity searches using patterns as seeds. *Nucleic Acids Res.* **1998**, *26*, 3986–3990. [CrossRef] [PubMed]
37. Huang, Y.; Niu, B.; Gao, Y.; Fu, L.; Li, W. CD-HIT Suite: A web server for clustering and comparing biological sequences. *Bioinformatics* **2010**, *26*, 680–682. [CrossRef]
38. Webb, B.; Sali, A. Comparative Protein Structure Modeling Using MODELLER. *Curr. Protoc. Bioinforma.* **2014**, *47*, 5.6.1–5.6.32. [CrossRef]
39. Pineda, T.; Churchich, J.E. Reversible unfolding of pyridoxal kinase. *J. Biol. Chem.* **1993**, *268*, 20218–20222.
40. Case, D.A.; Betz, R.M.; Cerutti, D.S.; Cheatham, T.E., III; Darden, T.A.; Duke, R.E.; Giese, T.J.; Gohlke, H.; Goetz, A.W.; Homeyer, N.; et al. AMBER 2016. University of California: San Francisco, CA, USA, 2016.
41. Maier, J.A.; Martinez, C.; Kasavajhala, K.; Wickstrom, L.; Hauser, K.E.; Simmerling, C. ff14SB: Improving the Accuracy of Protein Side Chain and Backbone Parameters from ff99SB. *J. Chem. Theory Comput.* **2015**, *11*, 3696–3713. [CrossRef]
42. Meagher, K.L.; Redman, L.T.; Carlson, H.A. Development of polyphosphate parameters for use with the AMBER force field. *J. Comput. Chem.* **2003**, *24*, 1016–1025. [CrossRef]

43. Gordon, J.C.; Myers, J.B.; Folta, T.; Shoja, V.; Heath, L.S.; Onufriev, A. H++: A server for estimating pKas and adding missing hydrogens to macromolecules. *Nucleic Acids Res.* **2005**, *33*, W368–W371. [CrossRef]
44. Roe, D.R.; Cheatham, T.E. PTRAJ and CPPTRAJ: Software for processing and analysis of molecular dynamics trajectory data. *J. Chem. Theory Comput.* **2013**, *9*, 3084–3095. [CrossRef] [PubMed]
45. Bradford, M.M. A rapid and sensitive method for the quantitation of microgram quantities of protein utilizing the principle of protein-dye binding. *Anal. Biochem.* **1976**, *72*, 248–254. [CrossRef]
46. Abercrombie, D.M.; Martin, D.L. Inhibition of pyridoxal kinase by the pyridoxal-gamma-aminobutyrate imine. *J. Biol. Chem.* **1980**, *255*, 79–84. [PubMed]
47. Storer, A.C.; Cornish-Bowden, A. Concentration of MgATP2- and other ions in solution. Calculation of the true concentrations of species present in mixtures of associating ions. *Biochem. J.* **1976**, *159*, 1–5. [CrossRef] [PubMed]
48. Castro-Fernandez, V.; Herrera-Morande, A.; Zamora, R.; Merino, F.; Gonzalez-Ordenes, F.; Padilla-Salinas, F.; Pereira, H.M.; Brandão-Neto, J.; Garratt, R.C.; Guixe, V. Reconstructed ancestral enzymes reveal that negative selection drove the evolution of substrate specificity in ADP-dependent kinases. *J. Biol. Chem.* **2017**, *292*, 15598–15610. [CrossRef] [PubMed]
49. Castro-Fernandez, V.; Bravo-Moraga, F.; Ramirez-Sarmiento, C.A.; Guixe, V. Emergence of pyridoxal phosphorylation through a promiscuous ancestor during the evolution of hydroxymethyl pyrimidine kinases. *FEBS Lett.* **2014**, *588*, 3068–3073. [CrossRef]
50. Reddick, J.J.; Kinsland, C.; Nicewonger, R.; Christian, T.; Downs, D.M.; Winkler, M.E.; Begley, T.P. Overexpression, purification and characterization of two pyrimidine kinases involved in the biosynthesis of thiamin: 4-amino-5-hydroxymethyl-2-methylpyrimidine kinase and 4-amino-5-hydroxymethyl-2-methylpyrimidine phosphate kinase. *Tetrahedron* **1998**, *54*, 15983–15991. [CrossRef]
51. McCormick, D.B.; Snell, E.E. Pyridoxal phosphokinases. II. Effects of inhibitors. *J. Biol. Chem.* **1961**, *236*, 2085–2088.